UNCLASSIFIED
SECURITY CLASSIFICATION OF THIS PAGE

REPORT DOCUMENTATION PAGE

DTIC FILE COPY

AD-A196 094

1b. RESTRICTIVE MARKINGS: None	
2b. DECLASSIFICATION/DOWNGRADING SCHEDULE: NA	3. DISTRIBUTION/AVAILABILITY OF REPORT: Approved for Public Release; distribution is unlimited.
4. PERFORMING ORGANIZATION REPORT NUMBER(S)	5. MONITORING ORGANIZATION REPORT NUMBER(S): AFATL-TR-88-71
6a. NAME OF PERFORMING ORGANIZATION: Aerodynamics Branch, Aeromechanics Division	6b. OFFICE SYMBOL (If applicable): AFATL/FXA
6c. ADDRESS (City, State, and ZIP Code): Air Force Armament Laboratory, Eglin Air Force Base, Florida 32542-5434	7a. NAME OF MONITORING ORGANIZATION
7b. ADDRESS (City, State, and ZIP Co	
8a. NAME OF FUNDING/SPONSORING ORGANIZATION	8b. OFFICE SYMBOL (if applicable)
8c. ADDRESS (City, State, and ZIP Code)	9. PROCUREMENT INSTRUMENT IDENTIFICATION NUMBER

DTIC ELECTE JUN 06 1988 S D C&D

10. SOURCE OF FUNDING NUMBERS			
PROGRAM ELEMENT NO.	PROJECT NO.	TASK NO.	WORK UNIT ACCESSION NO
62602F	2567	03	20

11. TITLE (Include Security Classification)

AEROACOUSTIC EFFECTS OF BODY BLOCKAGE IN CAVITY FLOW (UNCLASSIFIED)

12. PERSONAL AUTHOR(S)

Gates, Roger S.; Butler, Carroll B.; Shaw, Leonard L. (AFWAL/FIBG); Dix, Richard E.(AEDC/DOFX

13a. TYPE OF REPORT	13b. TIME COVERED	14. DATE OF REPORT (Year, Month, Day)	15 PAGE COUNT
Final	FROM Sep 86 TO Sep 87	87 October 19	9

16. SUPPLEMENTARY NOTATION

Paper presented at 11th AIAA Aeroacoustics Conference, 19-21 Oct 87, Palo Alto CA

17. COSATI CODES			18 SUBJECT TERMS (Continue on reverse if necessary and identify by block number)
FIELD	GROUP	SUB-GROUP	Generic Cavity Aeroacoustics
20	01		
01	02		

19. ABSTRACT (Continue on reverse if necessary and identify by block number)

In order to study the effects of unsteady (dynamic) and steady (static) pressure waves in a cavity at subsonic Mach numbers through transonic Mach numbers, an experimental test program, using a splitter plate and a generic cavity, was conducted. Since most cavities associated with air vehicles house sensors, equipment, or armament, ogive cylinder models were also fabricated and tested inside the cavity to determine their effect on the static and dynamic pressure measurements on the cavity ceiling and walls. The intent of the experiment was to document the effects on steady and unsteady pressures by varying parameters such as the Mach number, cavity dimensions, blockage, and cavity angle of attack. These results will provide engineers with a technology base to aid in the formulation of design requirements and preliminary designs for future air vehicles requiring external cavities.

20. DISTRIBUTION/AVAILABILITY OF ABSTRACT	21. ABSTRACT SECURITY CLASSIFICATION
☒ UNCLASSIFIED/UNLIMITED ☐ SAME AS RPT ☐ DTIC USERS	Unclassified

22a NAME OF RESPONSIBLE INDIVIDUAL	22b. TELEPHONE (Include Area Code)	22c OFFICE SYMBOL
Roger S. Gates	(904) 882-8410	AFATL/FXA

DD FORM 1473, 84 MAR — 83 APR edition may be used until exhausted. All other editions are obsolete.

SECURITY CLASSIFICATION OF THIS PAGE
UNCLASSIFIED

AEROACOUSTIC EFFECTS OF BODY BLOCKAGE IN CAVITY FLOW

Roger S. Gates*, Carroll B. Butler**
Aerodynamics Branch
Aeromechanics Division
Air Force Armament Laboratory
Eglin AFB FL 32542-5434

Leonard L. Shaw†
Structural Vibration Branch
Structures Division
Air Force Wright Aeronautical Laboratories
Wright-Patterson AFB OH 45433-6553

Richard E. Dix‡
Technology and Analysis Branch
Propulsion Wind Tunnel Facility
Calspan Corporation, AEDC Division
Arnold AFS TN 37389-9998

Abstract

In order to study the effects of unsteady (dynamic) and steady (static) pressure waves in a cavity at subsonic Mach numbers through transonic Mach numbers, an experimental test program, using a splitter plate and a generic cavity, was conducted. Since most cavities associated with air vehicles house sensors, equipment, or armament, ogive cylinder models were also fabricated and tested inside the cavity to determine their effect on the static and dynamic pressure measurements on the cavity ceiling and walls. The intent of the experiment was to document the effects on steady and unsteady pressures by varying parameters such as the Mach number, cavity dimensions, blockage, and cavity angle of attack. These results will provide engineers with a technology base to aid in the formulation of design requirements and preliminary designs for future air vehicles requiring external cavities.

Nomenclature

C_p	static pressure coefficient
dB	decibels
f	frequency
g	force of gravity
HZ	hertz, cycles per second
K	ratio of specific heats
L	cavity length
M	Mach number
m	mode number
P_{rms} psi	root mean squared pressure pounds per square inch
q	dynamic (head) pressure
SPL	sound pressure level
V	velocity
V_{rms}	root mean squared voltage
X	longitudinal position
Y	lateral position
Z	vertical position
∞	free stream

*Lt, USAF, Aeroballistics Section, Member AIAA
**Technical Advisor, Senior Member AIAA
†Aerospace Engineer, Acoustics and Sonic Fatigue Group, Member AIAA
‡Principal Research Engineer, Flight Dynamics Section, Senior Member AIAA

Introduction

It has previously been demonstrated that cavities located within a flow field can produce a severe aeroacoustic environment which is characterized by extremely high sound pressure levels.[1] The source of this aeroacoustic problem is believed to be a coupling between the unsteady separated shear layer (outside the open cavity) and the internal cavity wave structure.[2,3] This interaction can produce high modal amplitudes at discrete frequencies. These high sound pressure levels may in turn affect the performance of systems which operate within these cavities, particularly in the aft region of the cavity where the sound pressure levels are generally higher. A test to parametrically investigate the effects of cavity steady and unsteady pressures (including the addition of blockage in the cavity) was conducted in a 4-foot transonic wind tunnel over a Mach number range of M_∞ = 0.6 to 1.2. The aeroacoustic transient loads (also referred to as unsteady or dynamic pressures) were measured for a generic cavity at two length to depth ratio configurations. Data were obtained for an empty cavity and various conditions of blockage inserted inside the cavity. The blockage model was a generic ogive-cylinder configuration. A bent sting assembly was used to allow the body to move in and out of the cavity. This paper discusses the aeroacoustic effects of the following parameters: cavity length to depth ratio; longitudinal, lateral, and vertical cavity distributions; cavity angle of attack; Mach number/dynamic pressure variations; and variations of the body blockage location.

Test Articles and Instrumentation

This research was conducted in the 4-foot transonic wind tunnel at the Arnold Engineering Development Center. The support system for the splitter plate (with generic cavity) and blockage model is shown in Figure 1. Total blockage is approximately 1 percent of the wind tunnel cross sectional area. The flat plate portion of the cavity has a 15.2 degree

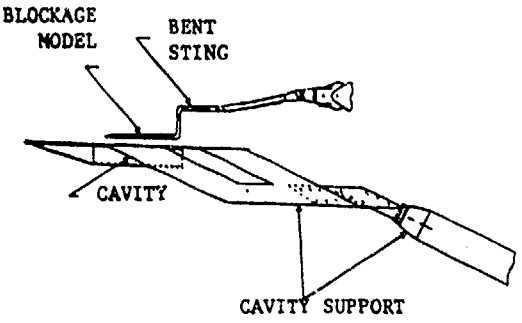

Fig. 1 Model support system.

beveled leading edge. The upstream wall (forward bulkhead) of the cavity was located 15 inches from the plate leading edge. The width and length of the cavity remained fixed at 4 and 18 inches respectively throughout the experiment. Two cavity depths (2 and 4 inches) were investigated, which provided length to depth ratios of 9.0 and 4.5 (Figure 2). The configuration which provided the blockage in the cavity was an ogive-cylinder body 0.7 inch in diameter and 14.4 inches long (Figure 3).

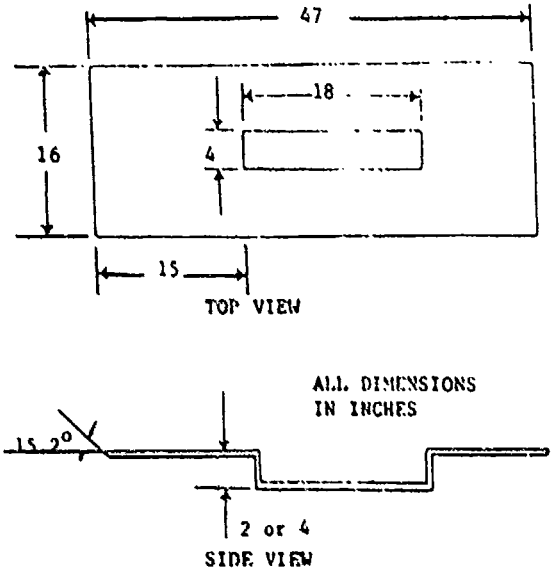

Fig. 2 Generic cavity dimensions.

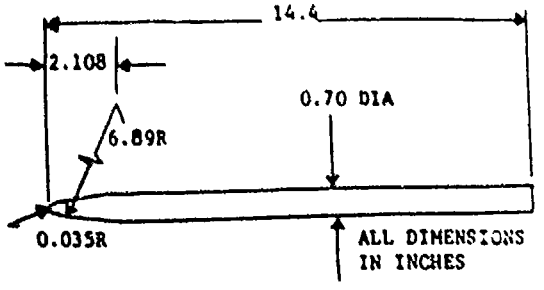

Fig. 3 Generic blockage model.

The unsteady pressure measurements were obtained using Kulite® Model XCS-093-50, 5 PSID pressure transducers (Figure 4). Thirty-three transducers were located in and around the cavity as shown in Figure 5. The unsteady data were recorded on magnetic tape and a single data point or record typically extended over a period of 10 to 15 seconds. A local tunnel timing code was used to synchronize the data on tape. Frequency analyses were performed on and off line with 25 HZ and 1 HZ filters, respectively.

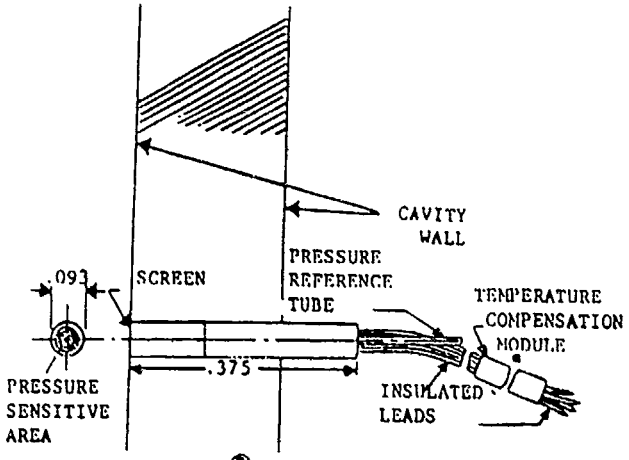

Fig. 4 Kulite® transducer sketch.

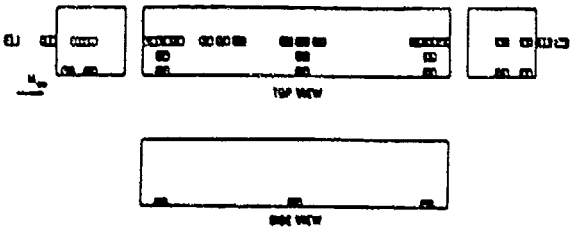

Fig. 5 Kulite® transducer locations.

Several of the unsteady pressure transducers were calibrated in the laboratory before the test. The transducer reference pressure lines were vented to the plenum areas around the cavity resulting in differential pressure measurements. A reference microphone was calibrated with several pistonphones at 250 Hertz and 124 dB sound pressure level (SPL). This reference microphone was then used to obtain transducer sensitivities at 140 dB SPL inside a high pressure calibrator. Before and after the test, a dynamic pressure calibration was applied to most transducers at 130 dB SPL with a pistonphone or 140 dB SPL with a power

amp and horn driver at a frequency of 250 Hertz. The tunnel amplifiers were set for 60 dB gain and the offline amplifiers were set for 0 dB gain. These calibrations were recorded on paper. The amplifiers were then normalized for 1 volt = 140 dB SPL before recording the calibration on tape. If the calibrator would not fit over the pressure transducer, the channel was normalized for 1 Vrms = 140 dB SPL. Calibrating the transducers inside the cavity was a little more difficult. A plate was fabricated to completely enclose the cavity, and when used with the power amp and horn driver, would simultaneously excite all transducers inside. This technique yielded an overall level of about 100 dB SPL. Nine channel frequency responses were checked by inserting random noise across the bridge outputs. This random noise was inserted into all the amplifier tracks simultaneously to check tape track skewness.

Accelerometers were calibrated on site using a three point (-1g, 0g, + 1g) static dump calibrator to determine the sensitivities. This calibration was recorded on tape.

SPL values were calculated using the following expression:

$$SPL\ (dB) = 20\ Log\ \frac{P_{rms}(psi)}{P_{ref}}\ 10^{9}$$

the assumed reference pressure is: 2.9008×10^{-9} psi.

Ninety-six surface transducers were used to obtain static pressures in the cavity and on the flat plate portion of the cavity. These pressures were measured by using two 48-port electronically scanned pressure modules mounted on the underside of the plate. Figure 6 shows the general location of the pressure orifices which are located on the cavity ceiling, bulkheads, sidewalls, and plate surfaces.

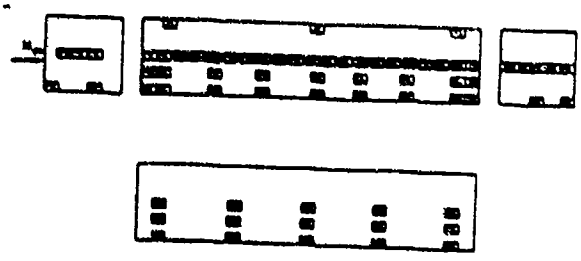

Fig. 6a Static transducer cavity locations.

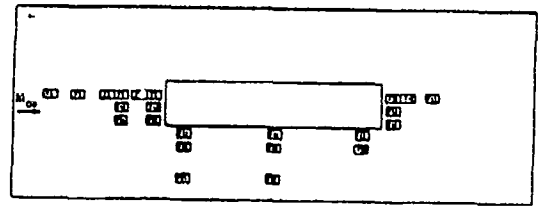

Fig. 6b Static transducer plate locations.

Other instrumentation included proximity sensors which provided measurement between the plate surface and blockage model support sting for accurate vertical positioning of the blockage model, four thermocouples attached to the interior wall surfaces of the cavity to measure the wall temperatures, and four hot film anemometers flush mounted at various distances from the plate leading edge (Figure 7). These anemometers were used to determine the type of boundary layer (laminar or turbulent) and the approximate location of transition. The boundary layer thickness at the upstream bulkhead can be calculated after the transition location is defined. This is important because the ratio of the boundary layer thickness to cavity depth is believed to have a major influence on the cavity acoustics. The two accelerometers were mounted on the underside of the plate assembly. These measurements (combined with the transient pressure readings) were used to determine if the vibration of the cavity support system was a significant component of the measured sound pressure level. One accelerometer was an Entran Model EGAL-125-100 located 6 inches from the leading edge. The other was a Setra Model 141A located on the aft bulkhead 1 inch from the cavity opening. The accelerometer near the leading edge measured the normal vibration while the aft one measured the axial vibration.

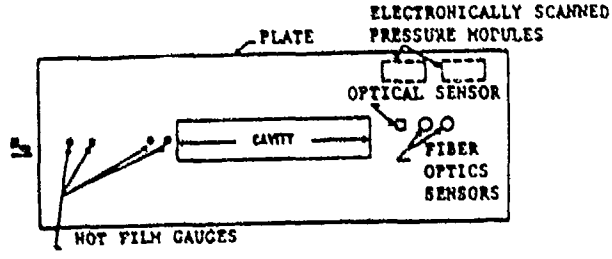

Fig. 7 Other cavity instrumentation.

Discussion of Results

Static Pressure Distribution

Typical static pressure distributions along the center line of the shallow and deep cavity are shown in Figure 8. This figure contains data from the cavity ceiling, forward and aft bulkheads, and positions on the plate upstream and downstream of the cavity. The X/L positions of 0 and 1 coincide with the forward and aft cavity bulkheads, respectively. A strong pressure gradient between the two curves was observed at $M_\infty = 0.60$, however, as the Mach number was increased to $M_\infty = 1.20$, it was not as pronounced. It is realized that the bent sting will affect the static pressure distribution in the cavity and around the base region of the blockage model. A detailed assessment of such sting effects will be accomplished in a future test entry that will include static and dynamic pressure instrumentation on the blockage model as well as the cavity.

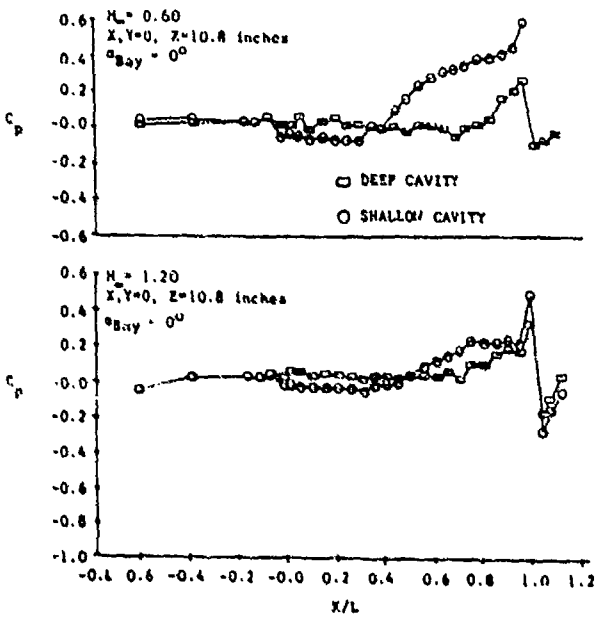

Fig. 8 Typical static pressure distributions.

Deep versus Shallow Bay Unsteady Pressure Levels

The effect of the cavity length to depth ratio is shown in Figure 9 for the K15 dynamic transducer located on the ceiling in the aft region of the cavity. The blockage model was placed inside the cavity at Z = -1.2 inches (Z = 0 inches would correspond to the lip of the cavity flush with the flat plate). This figure indicates that the shallow cavity effectively suppresses the strong tones that are associated with the deep cavity configuration. The data also indicate that the selected deep cavity configurations exhibit the classical open flow condition which is normally associated with deep cavities. Open flow is a condition where the on-rushing airstream bridges the gap formed by the forward and aft bulkheads. This contributes to the high sound pressure level modal peaks because of the acoustic energy trapped under the shear layer. A transitional state is indicated for the shallow cavity configuration since modal peaks remain well defined particularly at $M_\infty = 1.2$ where the peaks are 8 to 10 dB above the broadband levels. Closed flow is the condition where the airstream attaches to the cavity ceiling with the subsequent elimination of the modal peaks. In Figure 9 the modal peaks are well defined at the lower frequencies particularly for the deep cavity where they are at least 8 to 10 dB above the broadband levels. Broadband SPLs are similar for both the shallow and deep cavity.

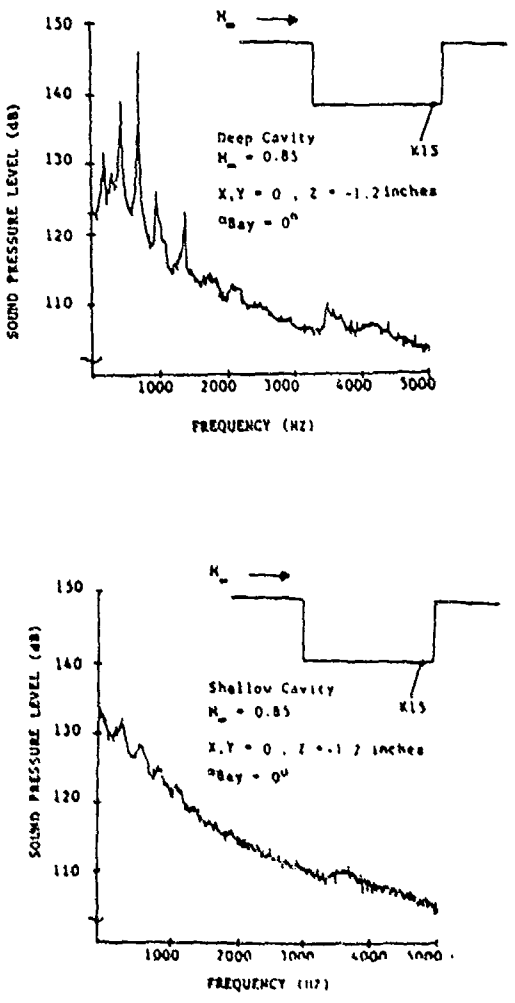

Fig. 9 Deep versus shallow cavity acoustics.

SPL Variation with Longitudinal Position in Cavity

These test results are consistent with previous experimental investigations such as those in Reference 4. A 10 dB increase in broadband levels was observed going from the front to the aft region of the cavity. Typical

deep cavity results are shown in Figure 10 for transducers K5, K12, and K16. In addition, the modal peak amplitudes exhibit significant variations as a result of the mode shapes of the standing waves in the deep cavity. Conversely, minimal modal frequency excitations were observed in the shallow cavity (not shown). Broadband sound pressure levels were generally observed to be similar in the aft region of the cavity for both shallow and deep cavities. In the mid region of the shallow cavity there were reduced sound pressure levels which are believed to be due primarily to the interaction between the boundary layer and the cavity.

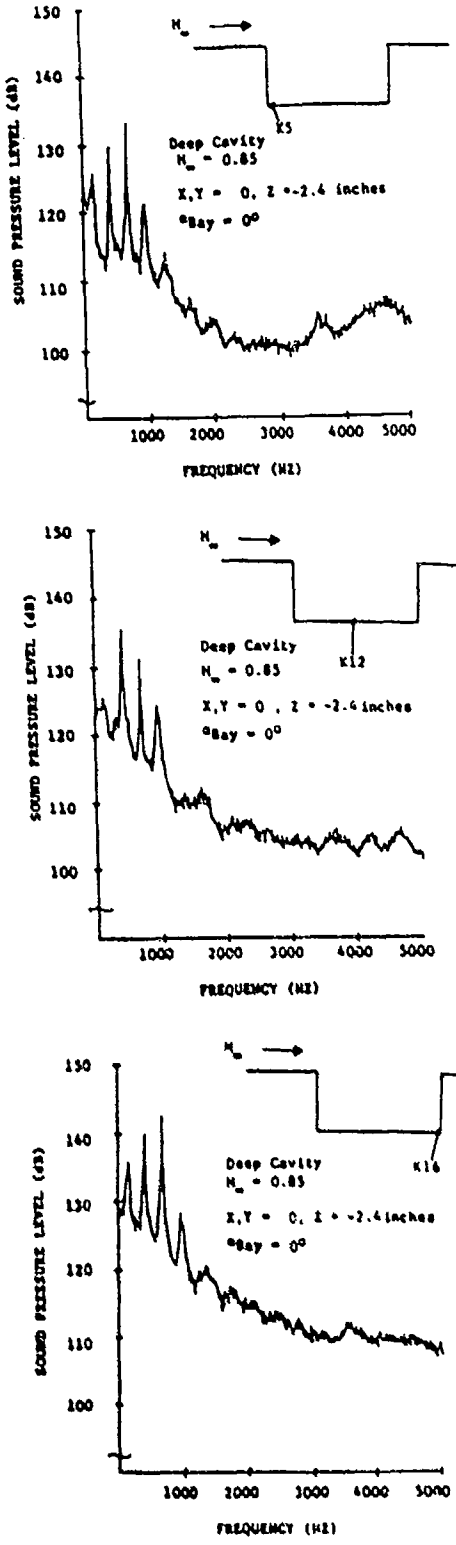

Fig. 10 Typical cavity longitudinal SPL distribution.

SPL Variation with Lateral Bay Position

The SPL variation with lateral position is shown in Figure 11 for the K15 and K28 transducers at $M_\infty = 0.85$. Minimal lateral variations in the resonant peaks were observed with only a 3 to 5 dB increase in SPL evident going from cavity centerline to the sidewall. Similar lateral variations were observed at other longitudinal locations. These trends were consistent over the entire Mach number regime for both cavity depths.

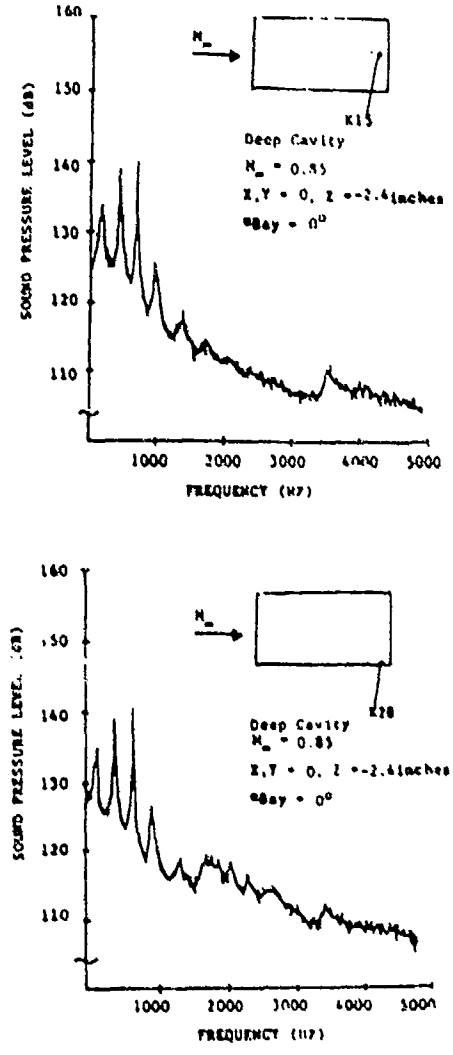

Fig. 11 Typical cavity lateral SPL distribution.

SPL Variation with Vertical Cavity Position

A typical vertical SPL variation is shown in Figure 12 for the K26 and K31 transducers in the forward portion of the cavity. A 3-4 dB increase in the modal peaks was generally observed moving from the ceiling to the lip of the cavity. In the aft portion of the cavity, minimal variations were observed on the sidewalls; however, 7-8 dB higher broadband levels were measured on the aft bulkhead near the lip of the cavity. Similar trends were observed throughout the test for both cavity depths.

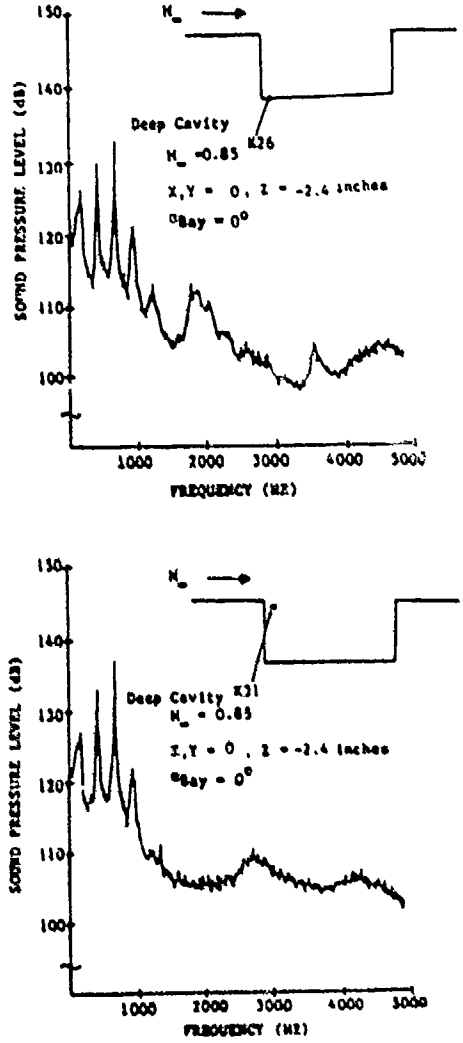

Fig. 12 Typical cavity vertical SPL distribution.

SPL Variation Upstream and Downstream of Cavity

Sound pressure levels for the K1 and K2 transducers are shown in Figure 13. The modal amplitudes for both the K2 and downstream K19 (not shown) transducers are similar to those measured in the cavity. The modal amplitudes up to 1000 HZ were significantly reduced as the transducer was located further away from the cavity (K1 and K20). The broadband tones observed from 2000-5000 HZ are believed to be related to wind tunnel induced noise sources such as the compressors and the perforations in the test section side walls. These broadband peaks were not observed inside the cavity as they were probably masked by the higher levels present. However, a consistent change in broadband levels was measured on transducers inside the cavity at approximately 3500 HZ.

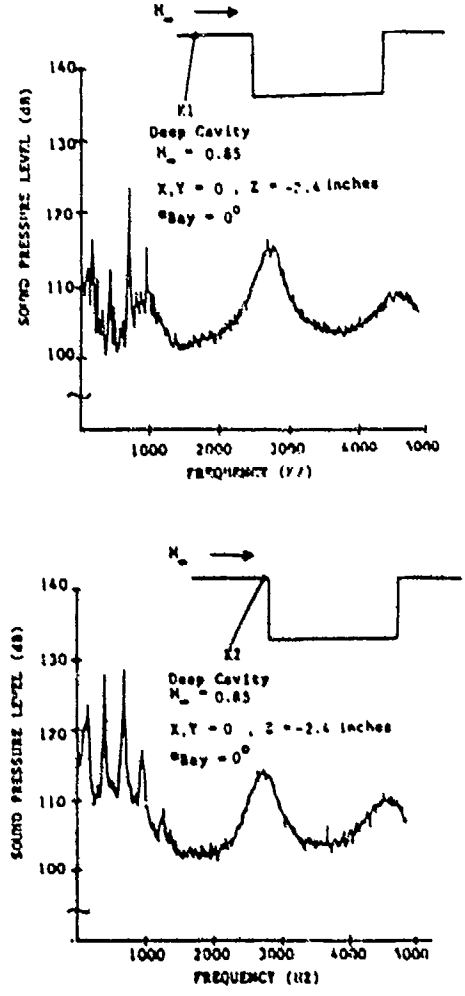

Fig. 13 Typical SPL distribution upstream of cavity.

Cavity Angle of Attack Effect

The effect of the cavity angle of attack at zero and 5 degrees is shown in Figure 14 for the K15 transducer. The effects on resonant frequency peaks and broadband levels are minimal for the shallow cavity (Figure 14a). However, a significant angle of attack effect was observed at M_∞= 0.95 for the deep cavity resonant frequency peaks as shown in Figure 14b with modes 2 through 5 attenuated about 8 dB. Broadband level changes were minimal for the deep cavity. In contrast, the angle of attack effect on the deep cavity was again minimal at M_∞= 1.20 as seen in Figure 14c. The cavity angle of attack was necessarily limited to 5 degrees to minimize total blockage effects in the test section. This relatively small angle of attack capability is a liability, however, alternatives are limited. Reducing the model scale is undesirable due to unfavorable scaling effects on acoustic data and testing in larger facilities is much more expensive.

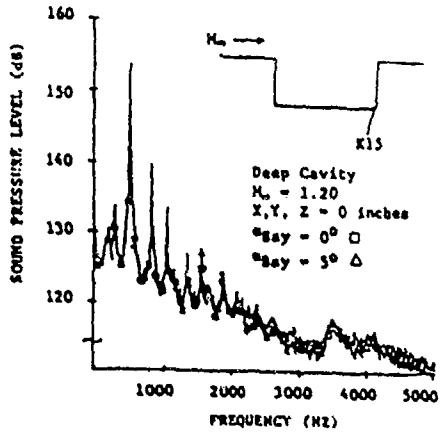

Fig. 14 Cavity angle of attack effect on SPL (concluded).

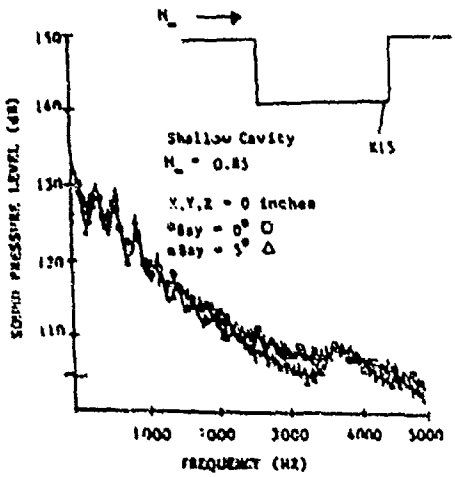

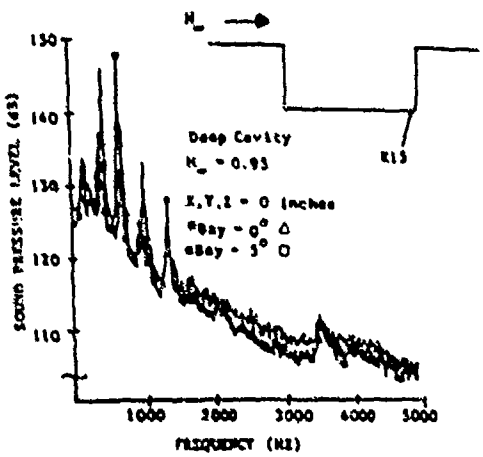

Fig. 14 Cavity angle of attack effect on SPL.

Mach Number Effect

The effect of Mach number variations is shown in Figure 15 for the deep cavity at M_∞= 0.60 and 1.20. The modal frequencies at narrowband peaks increase with increasing Mach number. These increases were predicted using the modified Rossiter equation as shown below.

$$F_m = \frac{\frac{V}{L}\frac{m - 0.25}{M}}{\left(1+\frac{K-1}{2}M^2\right)^{1/2} + 1.75}$$

Where V = Freestream velocity
M = Mach number
L = Cavity length
K = Ratio of specific heat
m = Modes; 1,2,3, etc
F = Frequency

The tic marks shown near the measured modal peaks show good agreement between the predicted and measured frequencies. Mode switching was observed for the deep cavity. For example, Mode 3 dominated up to M_∞= 0.85 switching to Mode 2 at higher Mach numbers. In contrast, modal amplitudes were generally lower for the shallow cavity configuration (not shown) and varied only slightly as the Mach number changed. It should be noted that wind tunnel dynamic pressure (q) also varies with Mach number.

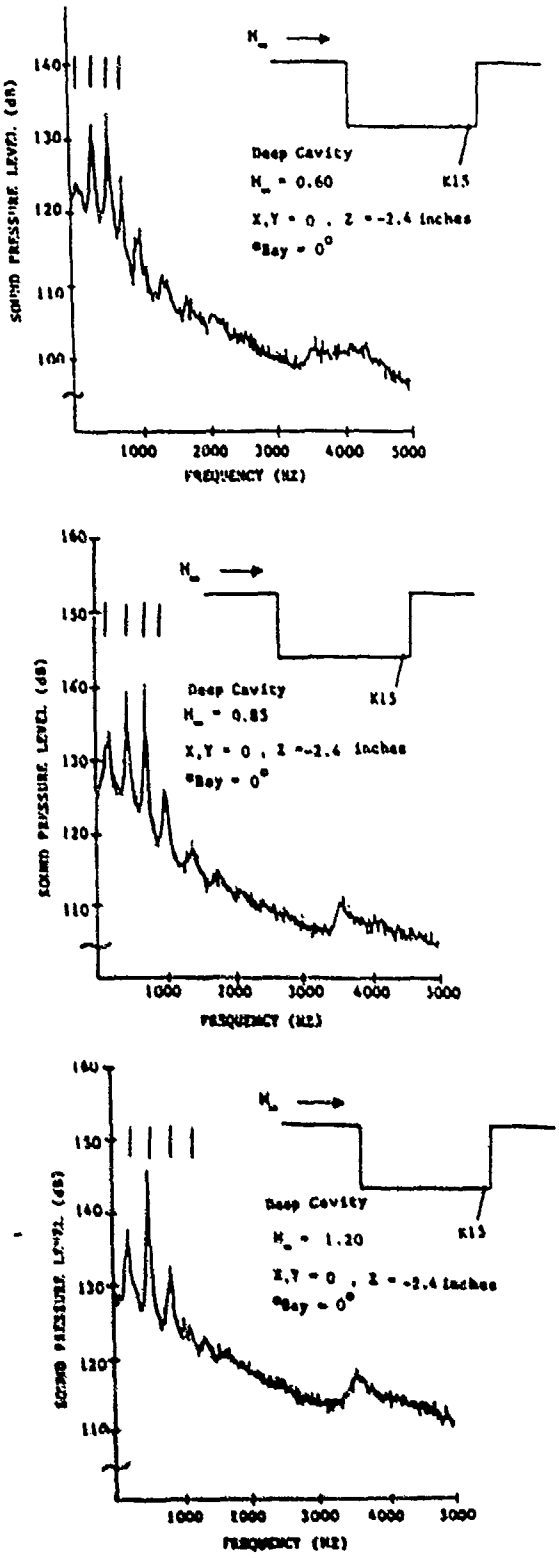

Fig. 15 Mach number/dynamic pressure effect on SPL.

Body Blockage Vertical Location Effects

The effect of body vertical location on SPL is shown in Figure 16 for the deep cavity. Broadband levels were generally insensitive to the blockage model location although some shifting of the modal frequency amplitudes was observed. For instance, mode 3 reached a peak at Z = -1.2 inches (blockage model inside the cavity) while modes 1 or 2 peaked at blockage model locations outside the cavity. These vertical location effects were minimal for Z greater than 2.4 inches.

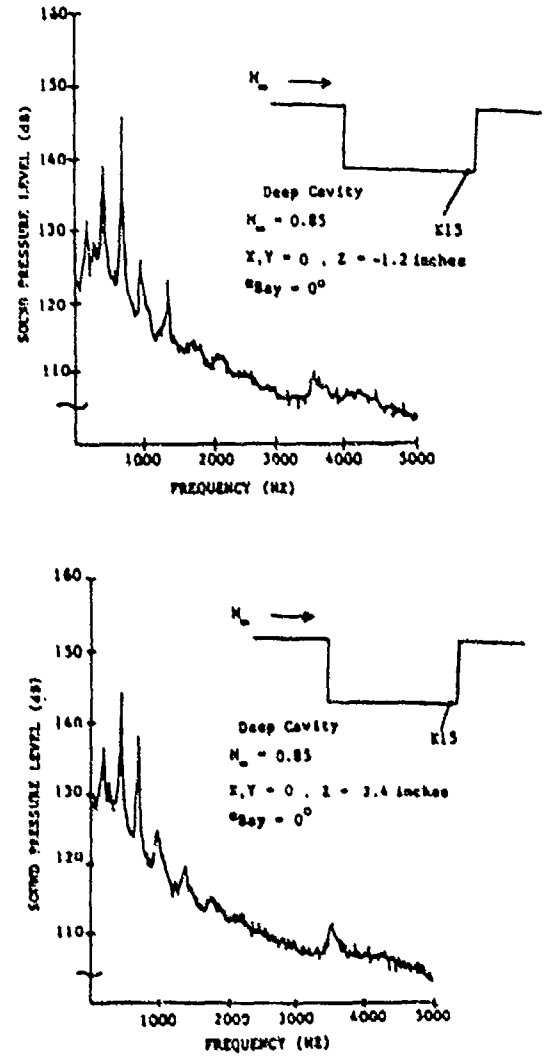

Fig. 16 Blockage model vertical location effect on SPL.

Body Blockage Longitudinal Location Effect

The effect of longitudinal forward and aft location of the blockage model just above the cavity opening (Z=1.2 inches) is shown in Figure 17 for the deep cavity at a M_∞= 0.85. The X location refers to the longitudinal position of the center of gravity the blockage model. Zero corresponds to the forward bulkhead with negative numbers indicating upstream positions and positive numbers indicating downstream locations. Broadband levels did not change as the model X position was varied; however, some sensitivity in modal frequency amplitudes was observed (3 to 5 dB).

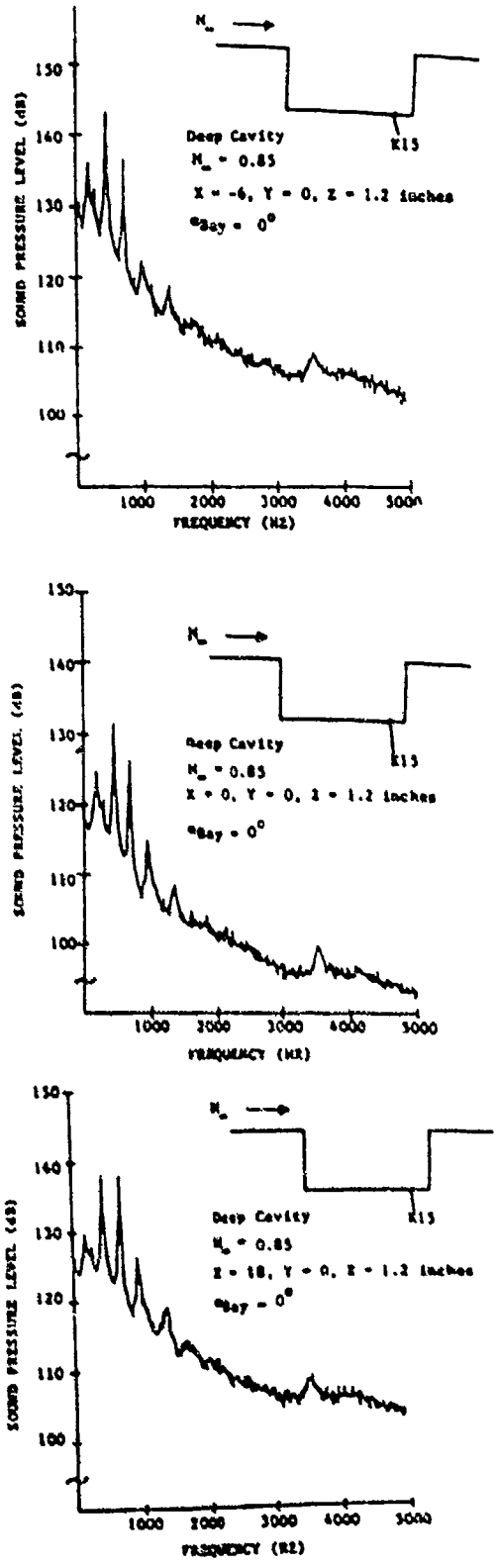

Fig. 17 Blockage model longitudinal location effect on SPL.

Conclusions

The results presented in this paper provide good agreement with the minimal amount of research conducted in the past. The value of this research is that it provides a more detailed and extensive data base for engineers to utilize during early stages of air vehicle design requiring the utilization of internal cavities. Additional tests are currently being planned which will extend this technology data base even further to include aeroacoustic suppressors, cavity doors, and supersonic Mach number effects. These results will be documented in subsequent reports.

References

1. Shaw, L., Clark, R., and Talmadge, D., "F-111 Generic Weapons Bay Acoustic Environment," AIAA-87-0168, January 1987.

2. Kaufman, L. G., Maciulaitis, A., and Clark, R. L., "Mach 0.6 to 3.0 Flows Over Rectangular Cavities", AFWAL-TR-82-3112, USAF, May 1983.

3. Marquardt, M. F., "An Experimental Investigation of Pressure Oscillation in Two-Dimensional Open Cavities", AFIT Thesis AD A023355, December 1975.

4. Smith, D. L., "Prediction of the Pressure Oscillations in Cavities Exposed to Aerodynamic Flow," AFFDL-TR-75-34.